JBC Papers in Press. Published on May 21, 2018 as Manuscript RA117.001698
The latest version is at http://www.jbc.org/cgi/doi/10.1074/jbc.RA117.001698

# A human-specific, truncated α7 nicotinic receptor subunit assembles with full-length α7 and forms functional receptors with different stoichiometries

**Matías Lasala, Jeremías Corradi, Ariana Bruzzone, María del Carmen Esandi and Cecilia Bouzat***

Instituto de Investigaciones Bioquímicas de Bahía Blanca, Departamento de Biología, Bioquímica y Farmacia, Universidad Nacional del Sur-Consejo Nacional de Investigaciones Científicas y Técnicas (CONICET), Bahía Blanca, Argentina.

***Running title**: dupα7 subunit function*

*To whom correspondence should be addressed at: Instituto de Investigaciones Bioquímicas de Bahía Blanca (INIBIBB), CONICET Bahía Blanca, Camino La Carrindanga Km 7, 8000 Bahía Blanca, Argentina. E-mail: inbouzat@criba.edu.ar

**Keywords:** nicotinic acetylcholine receptors, patch clamp, Cys-loop receptor, channel activation, ion channel, receptor structure-function, single-channel recording, alpha7 receptor.

## ABSTRACT

The cholinergic α7 nicotinic receptor gene, *CHRNA7*, encodes a subunit that forms the homopentameric α7 receptor, involved in learning and memory. In humans, exons 5-10 in *CHRNA7* are duplicated and fused to the *FAM7A* genetic element, giving rise to the hybrid gene *CHRFAM7A*. Its product, dupα7, is a truncated subunit lacking part of the N-terminal extracellular ligand-binding domain and is associated with neurological disorders, including schizophrenia, and immunomodulation.

We combined dupα7 expression on mammalian cells with patch clamp recordings to understand its functional role. Transfected cells expressed dupα7 protein, but they exhibited neither surface binding of the α7 antagonist α-bungarotoxin nor responses to acetylcholine (ACh) or to an allosteric agonist that binds to the conserved transmembrane region. To determine if dupα7 assembles with α7, we generated receptors comprising α7 and dupα7 subunits, one of which was tagged with conductance substitutions that report subunit stoichiometry and monitored ACh-elicited channel openings elicited by ACh in the presence of a positive allosteric α7 modulator. We found that α7 and dupα7 subunits co-assemble into functional heteromeric receptors, that at least two α7 subunits are required for channel opening, and that dupα7's presence in the pentameric arrangement does not affect the duration of the potentiated events compare with that of α7. Using an α7 subunit mutant, we found that activation of $(\alpha7)_2(\text{dup}\alpha7)_3$ receptors occurs through ACh binding at the α7/α7 interfacial binding site. Our study contributes to the understanding of the modulation of α7 function by the human specific, duplicated subunit, associated with human disorders.

α7 is a homomeric member of the nicotinic receptor (nAChR) family, which belongs to the pentameric ligand-gated ion channel superfamily (1–3). α7 receptors are localized in the central and peripheral nervous systems as well as in non-neuronal cells. They have pleiotropic effects ranging from the modulation of neurotransmitter release and the induction of excitatory impulses in the nervous system to the regulation of inflammatory responses in the immune system (4, 5). Decreased expression and function of α7 has been associated with neurological and neurodegenerative disorders, including Alzheimer's disease, schizophrenia, bipolar disorder, attention deficit hyperactivity disorder, autism spectrum disorder (6).

Nicotinic receptors contain a large extracellular domain, which carries the agonist binding site, a transmembrane region, which is formed by four transmembrane segments of each subunit (M1-M4) with the M2 domains forming the walls of the ion pore, and an intracellular region that contains sites for receptor modulation and determinants of channel conductance (3, 5). At the interface between the extracellular and transmembrane domains, several loops form a network that relays structural changes from the binding site toward the pore. This region, named as coupling region, contributes to the fundamental mechanism of receptor activation (7–9).

The acetylcholine (ACh) binding sites are located at the interfaces of the extracellular domains of adjacent subunits. Each binding site is composed of a principal face provided by one subunit, which contributes three loops, named A, B and C, and a complementary face provided by the adjacent subunit, which contributes Loops D, E and F (10, 11). The homomeric α7 receptor has five identical ACh binding sites; however, ACh occupancy of only one site is enough for activation (12).

The α7 receptor subunit gene, *CHRNA7*, has 10 exons and is located on the long arm of chromosome 15 (15q13-q14). A hybrid gene, *CHRFAM7A*, has arisen from a relatively recent partial duplication that comprises exon 5 to 10 of the *CHRNA7* gene and is positioned in the same chromosome, centromeric to the *CHRNA7* gene by 1.6 Mb, interrupting the genetic element *FAM7A*. Interestingly, the *CHRFAM7A* gene is human specific (6, 13, 14). The final protein, dupα7, is a truncated receptor subunit that lacks the first 95 amino acid residues of α7 protein, which includes Loops D and A of the agonist binding site, and instead contains 27 amino acid residues from FAM7A at the N terminal domain (15). The *CHRFAM7A* gene is located in a complex region on chromosome 15 that includes many segmental, highly variable, duplications that result in several different copy number variants (CNVs). These multiple polymorphisms are associated with the risk to develop several neurological and psychiatric disorders, such as schizophrenia, bipolar disorder, autism, and idiopathic epilepsies (16, 17). Among the CNVs present in chromosome 15, another variant truncated subunit gene has been described, which shows a 2bp deletion in exon 6 of the *CHRFAM7A*, which has been associated with schizophrenia and P50 sensory gating deficit (13, 16).

High expression of dupα7 also occurs on human leukocytes (17, 18). In primary monocytes and macrophages, lipopolysaccharide treatment down regulates the expression of dupα7 (19). These findings suggest that the duplicated isoform might have a role in the immune system and cholinergic anti-inflammatory pathway. It is also present in a great variety of epithelial cells, confirming a wide distribution of expression of this truncated subunit (20).

The dupα7 subunit has been expressed heterologously in mammalian cell lines and *Xenopus* oocytes in a few studies. Immunological studies in GH4C1 cells suggested that dupα7 can reach the cell periphery, although it appeared to be at an inner location than that of α7 (21). No macroscopic responses have been detected after exposure to α7 agonists (21, 22). The role of dupα7 remains unclear since reduction of α7 currents, compatible with a negative modulator role, has been shown in oocytes (21, 23) but not in neuronal cells (22). By incorporating fluorescent tags Wang *et al.* (22) proposed that dupα7 can assemble with the full length α7 since both subunits are membrane localized in close position. The stoichiometry of these hybrid receptors and their function remain unknown.

To find a way to identify the possible pentameric α7/dupα7 arrangements and to determine their functional signature, we combined cell expression and single-channel recordings with the electrical fingerprinting strategy (12, 24–26). Receptors were generated using combinations of α7

and dupα7 subunits, one of which carries a reporter conductance mutation that allows defining the subunit stoichiometry of the receptor that originated each single-channel opening event in real time. Our results provide novel information about the function of the duplicated α7 subunit, which may have a significant role in immunomodulation and in the pathophysiology of neurological disorders.

## Results

### *Heterologous expression of dupα7 on mammalian cells*

The cloned dupα7 cDNA includes the 1236-nucleotide sequence previously deposited in NCBI and corresponds to the *CHRFAM7A* isoform 1 (accession number NM_139320). The initiator methionine in exon B of *CHRFAM7A* will produce a protein including amino acid residues coded by part of exon B, exon A of the *FAM7A* gene and exons 5–10 of *CHRNA7* (Fig. 1A). The final protein contains the N-terminal domain with 27 residues of *FAM7A* followed by α7 sequence starting at amino acid residue 96 and therefore lacks loop A and D of the ACh-binding site (Fig. 1A).

To establish that the cloned dupα7 cDNA is translated into the truncated subunit in our system, BOSC-23 cells were transfected with plasmid vectors containing either dupα7 or α7 cDNAs together with plasmids encoding the chaperone proteins, Ric-3 and NACHO in a 2:1:1 molar ratio, respectively. The expression of α7 and dupα7 subunit proteins was detected by western blotting from whole cell lysates using a previously characterized antibody raised against the intracellular M3-M4 loop that is common to both subunits (27). Western blot revealed bands in the range of 55-57 kDa in α7 expressing cells and in a lower molecular weight range (45-50 kDa) in those transfected with dupα7 cDNA. These bands, which were not detected in non-transfected cells, are compatible with the expected molecular weights of both subunits (Fig. 1B; (18, 19)). Double bands as the ones observed have been described before for α7 and might represent forms differing in glycosylation or in other post-translational modifications (28–30). Thus, our western blotting results confirm that dupα7 is transcribed and translated in our heterologous expression system.

### *dupα7 reduces the number of α-BTX binding sites when co-expressed with α7*

To detect the presence of surface receptors, transfected cells were labelled by Alexa Fluor 488-α-BTX, a selective α7 antagonist, and examined by confocal microscopy. The confocal images showed high level of expression of α7 but no binding of Alexa Fluor 488-α-BTX to cells expressing dupα7 as described before (21) (Fig. 2). Analysis of membrane fluorescence intensity revealed reduced fluorescence in cells that co-expressed dupα7 with α7 (α7:dupα7 1:3 cDNA subunit ratio) with respect to those expressing α7 (Fig. 2).

### *dupα7 does not mediate functional responses elicited by α7 orthosteric or allosteric agonists*

To examine function, α7 or dupα7 were expressed in BOSC-23 cells and examined by single-channel recordings. In the presence of 100-500 μM ACh, α7 exhibits single brief openings (~0.25 ms) flanked by long closings, or less often, few openings in quick succession, known as bursts (Fig. 3A, Table 1, (5, 12, 31)). Positive allosteric modulators (PAMs), such as the type II PAM PNU-120596 (32,33), are used as tools for increasing the probability of channel opening of α7. By slowing the onset of α7 desensitization and trapping activated α7 channels in an open conformation, PNU-120596 facilitates the detection of infrequent opening events and, at the same time, allows the accurate registering of their amplitudes (Fig. 3B, (34–35)). In cells expressing α7, ACh in the presence of PNU-120596 (1 μM) elicited long duration openings separated by brief closings, grouped in bursts, which in turn coalesce into long activation periods, clusters (~1-3 s) (Table 1, Fig. 3B, (32)). The open duration histogram is well fitted by three exponential components (Table 1, Fig. 3B). Neither clusters nor isolated openings were detected in the presence of 100 μM ACh and 1 μM PNU-120596 from cells transfected with dupα7 cDNA together with Ric-3 and NACHO (n=23 recordings from 4 different cell transfections, Fig. 3B), in agreement with the lack of macroscopic responses previously reported (21, 22). These experiments were performed in parallel with single-channel recordings from cells of the same batch transfected under identical conditions with α7 cDNA to confirm successful transfection and receptor expression. As an additional control, we performed recordings from cells transfected only with Ric-3 and NACHO cDNAs and showed no

channel activity elicited by ACh and PNU-120596 (n=8).

Since dupα7 lacks Loops A and D of the agonist binding site we sought to explore activation by an α7 allosteric agonist, 4BP-TQS, which binds to the transmembrane region that is conserved between α7 and dupα7 (36). The underlying hypothesis is that if the absence of Loops A and D of the ACh binding site were the cause of the lack of response, this should be overcome by using a ligand that activates from a conserved site. In α7, 10-50 μM 4BP-TQS elicits prolonged opening events (65 ± 24 ms, n=5) grouped in very long duration clusters (1539 ± 682 ms, n=5) (Fig. 3C). Macroscopic currents elicited by this allosteric agonist decay more slowly than those elicited by ACh (Fig. 3D, (36)). Neither single-channel currents (12 patches from 3 different cell transfections) nor macroscopic responses (12 cells from 3 different transfections) elicited by 4BP-TQS were detected from cells expressing dupα7 (Fig. 3C and 3D). Thus, we conclude that dupα7 cannot form functional receptors.

***Functional α7/ dupα7 heteromeric receptors***

In principle, possible co-assembly of α7 and dupα7 could be determined by co-expressing both subunits. However, single-channel activity derived from the homomeric α7 will probably be the predominant one and functional individual heteromeric arrangements will be indistinguishable. What is needed is a means to unequivocally distinguish functional heteromeric receptors and to directly associate channel openings to heteromeric α7/dupα7 receptors of a given stoichiometry. Thus, to determine if the co-assembly of dupα7 and α7 subunits leads to functional receptors and to establish the stoichiometry of the functional heteromeric arrangements, we applied the electrical fingerprinting strategy. The strategy is based on the combined expression of α7 with an α7 subunit mutant that contains three arginine substitutions at the intracellular M3-M4 loop region (α7LC for α7 low conductance, Fig. 4 top). Although α7LC receptors are functional as evidenced by macroscopic current recordings, single channels cannot be detected because the amplitude is reduced to undetectable levels (12, 24–26, 37). Because of the brief duration of α7 channels, openings events cannot be fully resolved due to filter bandwidth limitations. Thus, the strategy needs to be performed in the presence of a modulator, here PNU-120596, that by increasing open channel lifetime allows accurate measurements of channel amplitude (35). Recordings of α7 in the presence of 100 μM ACh and 1 μM PNU-120596 showed a homogeneous amplitude population of 9.8 ± 1.7 pA (-70 mV membrane potential; n=5 patches from 3 different cell transfections) for both individual opening events and clusters (Fig. 4A, Table 1). Under the same recording conditions, single channel openings from α7LC receptors were not detected due to their low amplitude (Fig. 4B). When α7LC was expressed together with α7 (1:4 for α7:α7LC cDNA subunit ratio), instead of the homogenous amplitude population of clusters detected for α7 alone, clusters of different amplitudes were observed (Fig. 4C). Clusters can be grouped into different amplitude classes, which can be well distinguished from the amplitude histograms (Fig. 4C and 5A). Studies from our and other labs have shown that the different amplitude populations report the number of low conductance subunits in each type of pentameric arrangement (12, 26, 37). Thus, amplitude classes of clusters of ~ 4-, 6-, 8- and 10-pA (-70 mV membrane potential) correspond to receptors containing 3, 2, 1 and 0 α7LC subunits, respectively (Fig. 5A, (12)). In previous studies we also analyzed a 2-pA class that corresponds to receptors containing 4 α7LC subunits (12). Here, information from this class was obtained using the reverse combination (see below).

Clusters in the presence of ACh and 1 μM PNU-120596 were not detected from cells transfected with α7LC cDNA (Fig. 4B) (n=19 of 4 different transfections, and (12)) or with dupα7 cDNA (Fig. 4D, n=23). In contrast, they were detected from cells expressing both subunits (α7LC:dupα7 1:3, 1:4 and 1:6 cDNA subunit ratios) (Fig. 4E). This result unequivocally indicates that dupα7 assembles with α7LC. It is important to note that the frequency of the active patches was markedly lower than that observed for the combination α7LC/α7. Under similar transfection conditions, 31% of cell patches showed channel activity in cells co-transfected with α7LC and dupα7 cDNAs (53 out of 171 patches) whereas this percentage increased to about 80% in cells transfected with α7LC and α7 cDNA.

The analysis of the amplitudes of clusters obtained from recordings of cells expressing the combination α7LC/dupα7 showed two predominant

classes whose mean amplitude values were 4.2 ± 0.3 and 5.8 ± 0.5 pA (Fig. 5B). In these recordings, we did not analyze the lowest 2-pA amplitude class, which would correspond to receptors containing one dupα7 subunit since channels of this stoichiometry were better detected using the reverse subunit combination (see below). In 27 % of the patches, a few clusters of higher amplitude were detected whose origin remains unknown. Because dupα7 conserves the portal amino acid residues responsible for α7 conductance, we can infer that the relationship between mean amplitude of each class and receptor stoichiometry is for dupα7/α7LC the same as for α7/α7LC. Thus, we can ensure that the detected 6- and 4-pA amplitude classes in the combination α7LC/dupα7 correspond to heteromeric receptors containing three and two dupα7 subunits, respectively (Figs. 4E and 5B).

To determine if heteromeric receptors containing only one dupα7 subunit are functional and to further confirm that the three portal amino acid residues in dupα7 govern channel amplitude, we introduced the triple mutation (RRR) in dupα7 to generate a low conductance dupα7 subunit (dupα7LC). We next transfected BOSC-23 cells with the combination α7/dupα7LC (1:8 cDNA subunit ratio) and recorded single-channel currents in the presence of 100 µM ACh and 1 µM PNU-120596. The amplitude of the majority of clusters in all active patches was ~10 pA, which corresponds to that of homomeric α7 receptors, indicating the prevalence of this receptor over heteromers. However, clusters of lower amplitude, which were not detected in cells transfected with α7 alone, were detected. The analysis showed clusters of 10-, 8-, and 6 pA-amplitude classes (Fig. 4F), which correspond to receptors containing zero, one and two dupα7 subunits, respectively. In these experiments, we did not analyze amplitude classes lower than 6 pA, since the corresponding populations were well detected with the reverse combination (α7LC/dupα7) (Fig. 4E).

Thus, the application of the electrical fingerprinting strategy revealed that dupα7 can assemble with α7 forming functional heteromeric receptors containing one, two or three dupα7 subunits.

### *Arrangement of $(\alpha7)_2(dup\alpha7)_3$ receptors*

The ACh binding site is located at subunit interfaces (Fig. 6A). A conserved tyrosine (Y93) located in Loop A of the principal face of the binding site has been shown to be essential for channel activation (38). Since dupα7 lacks Y93 (See below), it is likely that it cannot contribute to an activable principal face. We explored if it contributes to the complementary face of the binding site although it lacks Loop D. Two possible pentameric arrangements containing three dupα7 and two α7 subunits may be formed depending whether the two α7 subunits are adjacent or not (Fig. 6B). If the two α7 subunits were not consecutive, activation would occur through the α7/dupα7 interface where dupα7 should provide an activable complementary binding-site face. To test this hypothesis, we co-expressed dupα7 with an α7 subunit carrying a mutation at Loop D of the complementary face of the binding site (α7W55T). We have previously shown that ACh does not elicit either single-channel nor macroscopic currents from cells expressing α7W55T receptors (Fig. 6C, (12, 24)). We did not detect any channel activity elicited by 100 µM ACh in the presence of 1 µM PNU-120596 from cells transfected with the combination α7W55T/dupα7 (subunit ratios 1:3 and 3:1, n=10 patches from three different cell transfections) (Fig. 6C). These results indicate that the complementary face of the binding site has to be provided also by the α7 subunit to allow activation. Thus, activation of α7/dupα7 heteromeric receptor occurs through the α7/α7 interfacial binding site. In consequence, in the pentameric $(\alpha7)_2(dup\alpha7)_3$ arrangement, the two α7 subunits are located consecutively.

Finally, we explored if channel kinetics elicited by 100 µM ACh in the presence of 1 µM PNU-120596 of $(\alpha7)_2(dup\alpha7)_3$ receptors are different to those of α7. To this end, we analyzed the 6-pA amplitude class of channels recorded from cells expressing α7LC and dupα7, which corresponds to receptors containing three dupα7 subunits, $(\alpha7LC)_2(dup\alpha7)_3$ (Fig. 4E and 5B). We found that the mean duration of the slowest open component and the mean cluster duration were not statistically different from those of α7 or of $(\alpha7LC)_2(\alpha7)_3$ obtained from the 6-pA population of the combination α7LC/α7 (Table 1). This analysis indicates that the truncated subunit does not alter the channel kinetics of potentiated receptors.

## Discussion

The expression and function of human α7 can be regulated at different stages and by different mechanisms, such as gene regulation through transcriptional mechanisms (6), co-expression of chaperone proteins (39, 40), receptor upregulation (41), interaction with intracellular proteins (42), and allosteric modulation by endogenous compounds (43). Another mechanism of potential modulation involves the partial duplication of the parent gene, an event which is evolutionary new and human specific (6, 44). The mechanism underlying such modulation and the physiological role of the truncated α7 subunit remain unknown.

To explore if the truncated subunit resulting from gene duplication, dupα7, modulates α7 function, we generated a dupα7 cDNA, expressed it on mammalian cells, and deciphered receptor function by single-channel recordings. By using a novel electrophysiological strategy, our results revealed that: i) dupα7 alone does not form functional ion channels; ii) dupα7 subunit can assemble with α7 forming a variety of heteromeric α7/dupα7 receptors; iii) for functional heteromeric α7/dupα7 receptors, at least two α7 subunits are required; iv) activation of heteromeric receptors requires an α7/α7 interfacial binding site, and; v) the kinetic signature of potentiated α7 receptors is not affected by dupα7.

Western blot using an antibody against the α7 intracellular loop, which is conserved between α7 and dupα7, showed that dupα7 cDNA is well translated in BOSC-23 cells. No α-BTX binding was detected in cells transfected with dupα7 cDNA, in agreement with previous results obtained in oocytes (21). Although no α-BTX binding was observed, heterologous expression of dupα7 homomers in the rat cell line GH4C1 as well as in oocytes was detected using an α7 antibody (21). However, it was described that such expression appeared to be at a more inner location than that of α7, probably within the endoplasmic reticulum (21). Although the probable absence of a signal peptide of the truncated protein suggests a subcellular localization, whether dupα7 homomers are present at the surface remains undefined. It is here important to note that a specific dupα7 antibody, which would facilitate its detection, is still not available.

It has been previously shown that the presence of dupα7 reduced significantly the number of α7 receptors in oocytes (21) but not in neuronal cells (22). However, in the latter system poor dupα7 translation was reported. In our system, overexpression of dupα7 (3-fold higher cDNA amount than α7 cDNA) reduced α-BTX-binding at the membrane level. However, we acknowledge that the level of reduction of fluorescence mediated by the presence of dupα7 may not be accurately determined due to possible bias introduced during the selection of fluorescent cells. In addition, only cells showing membrane fluorescence were analyzed. Assuming that translation and assembly are similar between α7 and dupα7 subunits, the binomial distribution indicates that 23% of the receptors should be dupα7 homomers and 39.5 % should contain only one α7 subunit in cells transfected with 1:3 α7:dupα7 cDNA subunit ratio. Under this scenario, an important reduction in α-BTX binding should occur since more than 60% of the receptors would not bind α-BTX and the rest would contain a reduced number of binding sites.

It is important to note that although we used Ric-3 and NACHO as chaperones, their actions on dupα7 as well as the most appropriate α7 subunit:chaperone ratio remain unknown. Also, the expression of dupα7 appears to depend on the cell type, i.e. in neurons the dupα7:α7 protein ratio is opposite to that in immune cells, dupα7 being the major product in the latter cells (17). Thus, this negative modulation of dupα7 on α7 expression observed in heterologous system might not be straightforward extrapolated to native systems.

Cells expressing only dupα7 did not show any detectable single-channel activity elicited by ACh in the presence of the potent PAM PNU-120596. This result supports the consensus that dupα7 does not form functional receptors in oocytes and mammalian cells (21, 22). A hypothesis in support of the absence of response is the lack of an intact ACh-binding site. To overcome the lack of an intact orthosteric agonist binding site, we used the α7 allosteric ligand, 4BP-TQS, which binds to the transmembrane region that is conserved between α7 and dupα7 (36). This ligand mediated strong responses in α7 but did not elicit neither macroscopic nor single-channel currents in cells expressing dupα7. These results confirm the absence of functional dupα7 receptors, which could arise from either the absence of dupα7 homomeric receptors in the membrane or from their inability to function as an ion channel.

To gain further insights into why the truncated subunit cannot form functional channels, we modeled dupα7 using I-TASSER server (45) (Fig. 7). Interestingly, the FAM7A peptide superimposed with loop A in the α7 structural model. However, in dupα7 this region lacks Y93, which is required for α7 activation (38). Also, the model shows the lack of Loop D at the complementary face, which carries W55 that is important for α7 function (25). Moreover, the lack of functional dupα7 channels is expected since this subunit also lacks the β1β2 loop (Fig. 7), which is located at the coupling region and is required for channel opening (7-9).

The electrical fingerprinting strategy has been extensively used for determining functional stoichiometry of α7-containing receptors (12, 26, 35, 37). This strategy requires the accurate measurement of channel amplitude, which acts as the reporter of the stoichiometry of each receptor that originated a single opening event or cluster. Given the brief open-channel lifetime of α7, the strategy needs to be performed in the presence of a PAM that by increasing open duration allows full channel amplitude resolution (12, 35). We chose PNU-120596 because it binds to a site that is conserved between α7 and dupα7 and at the same time it greatly increases opening probability thus facilitating functional detection of low-expressing receptors (46).

The α7LC carries a triple mutation in determinants of channel conductance, which are located at the loop between M3 and M4 transmembrane segments at the intracellular end of the ion channel (7, 47, 48). The triple mutation does not affect single-channel kinetics and only decreases α7 channel amplitude to undetectable levels (12, 24). As described in previous studies (12, 26, 37), when α7LC was co-expressed with α7, multiple and discrete amplitude classes were detected, each one corresponding to a different population of receptors with a fixed number of low conductance subunits. When instead of α7, dupα7 was expressed with α7LC, clusters of different amplitudes activated by ACh in the presence of PNU-120596 were detected. This result unequivocally indicates the presence of surface α7LC/dupα7 functional receptors since no channel activity was detected with either of the two individual subunits. The application of the electrical fingerprinting strategy revealed that dupα7 can assemble with α7 forming functional heteromeric receptors composed of one, two or three dupα7 subunits.

Since Loop A with its key tyrosine (Y93) is missing in dupα7 we infer that in the α7/dupα7 heteromers the α7 subunit should provide the principal face of the binding site. The lack of functional responses from cells expressing dupα7 and α7W55T, which does not contain a functional complementary face of the binding site, indicates that this face must be also provided by α7. Thus, in $(\alpha7)_2(dup\alpha7)_3$ receptors, the two α7 subunits are located consecutively and activation takes place through agonist binding at their interface. The fact that $(\alpha7)_2(dup\alpha7)_3$ can be activated despite carrying only one intact agonist binding site is in close agreement with our previous results showing that only one functional ACh binding site is sufficient for α7 activation and that the four additional sites increase ACh sensitivity (12). It also agrees with reports of α7β2 receptors showing that activation of this heteromeric receptor takes place through the α7/α7 interface (49, 50). Thus, it appears that in α7-heteromeric receptors at least one α7/α7 interfacial binding site is required for function.

We also showed that the mean durations of channel openings and clusters of $(\alpha7)_2(dup\alpha7)_3$ elicited by ACh in the presence of PNU-120596 are identical to those of α7, indicating that, at least in PNU-120596-potentiated receptors, the kinetics are not affected by dupα7. Unfortunately, this strategy cannot be performed in the absence of a potentiator due to the lack of full amplitude resolution and the low frequency of opening events (35).

Overall, our electrophysiological results predict that dupα7 will functionally operate as a negative modulator of α7 activity. Heteromers containing four dupα7 subunits are nonfunctional and those with three or less dupα7 subunits, despite being functional, have reduced ACh sensitivity due to the reduced number of active ACh binding sites (12, 25). An additional negative modulatory action of dupα7 might be associated with the decrease of the number of surface α7 receptors (21). However, this may differ between native and heterologous systems due to differences in gene expression, cell surface translocation, channel assembly or chaperones. Thus, our findings encourage to explore the assembly of heteromers in different human tissues.

Our study has been focused on ionotropic responses. However, α7 has been shown to act as a dual ionotropic/metabotropic receptor (5, 42). Considering that α7 channel-independent signal transduction is important in anti-inflammatory responses and that immune cells show high expression of dupα7 (17), it will be interesting to determine if the metabotropic activity differs between homomeric and α7/dupα7 heteromeric receptors.

From a molecular point of view, our findings provide novel information regarding α7 unique activation, and from a physiological point of view, they help to reveal the still unknown impact of the human-specific truncated subunit on α7 function.

## Experimental procedures

***Cloning of dupα7 cDNA.*** The full-length *CHRFAM7A* (variant 1: NM_139320.1) cDNA that encodes a 27-amino-acid terminus corresponding to FAM7A sequence (NH2-MQKYCIYQHF QFQLLIQHLWIAANCDI) and thereafter α7 sequence starting at ADERFDA, which corresponds to the end of Loop A of the binding site, was synthesized de novo (Biomatik, USA) with appropriate flanking restriction sites, XbaI and HindIII, for subcloning into the pUC19 plasmid to generate pUC19-dupα7. The dupα7 cDNA was excised from pUC19-dupα7 and subcloned into the cytomegalovirus-based expression vector pRBG4 (51). After cloning, the sequence of dupα7 cloned in pRBG4 was confirmed by DNA sequencing using capillary electrophoresis (Instituto de Biotecnología CICCVyA, INTA, Argentina).

***Site directed mutagenesis*.** Mutations were generated using the QuikChange® Site-Directed Mutagenesis kit (Agilent, UK)**.** The low conductance form of human α7 (α7LC) or dupα7 (dupα7LC) contained three mutations at the intracellular loop (Q428R, E432R, S436R (12)).

***Cell expression:*** BOSC-23 cells, derived from HEK 293 cells (51), were transfected by calcium phosphate procedure with dupα7 and/or human α7 cDNA (also subcloned in pRBG4 vector), essentially as described previously (52, 53). For the combinations α7LC:dupα7 and α7:dupα7LC the cDNA subunit molar ratios ranged between 1:3 to 1:10 to ensure the incorporation of dupα7 into the heteromeric receptor. Although the cDNA subunit ratio is not directly proportional to the subunit stoichiometry of the final receptor, an excess of one subunit over the other is expected to compensate for less efficient translation or assembly and to bias the receptor population toward pentamers with an excess of the surplus subunit (24, 54). Plasmids harboring cDNAs of the α7 chaperone proteins Ric-3 and NACHO were incorporated in all transfections (39, 55).

***Confocal fluorescence microscopy.*** Cells were plated on 12 mm glass coverslips in 35 mm dishes. They were transfected with α7 cDNA (0.3 μg), dupα7 cDNA (0.9 μg) or with the combination (1:3) of α7 (0.3 μg) and dupα7 (0.9 μg) cDNAs. Ric-3 (1 μg) and NACHO (1 μg) cDNAs were included during the transfection in all conditions. Mock transfected cells correspond to cells transfected with irrelevant plasmid DNA (1.2 μg). The total amount of DNA per transfection was normalized with the addition of irrelevant plasmid DNA. After 72 h, cell surface receptor labeling was carried out by incubating with α-BTX Alexa Fluor 488 conjugate (Molecular Probes) at a final concentration of 1 μg/ml for 1 hour in chilled DMEM medium. Cells were then fixed with 4% paraformaldehyde. Cultures were then analyzed by phase and fluorescence microscopy, using a Nikon Eclipse E600 microscope and by laser scanning confocal microscopy (LSCM; Leica DMIRE2) with a 20x objective. Fluorescence intensity, expressed as arbitrary units, was measured after manually outlining regions of interest (ROI) with the software ImageJ (National Institutes of Health, Bethesda, MD). The maximum fluorescence intensity of a given region of interest was measured within α-BTX-positive region of the cell surface, and the maximum fluorescence intensity of an area of the same size positioned over a α-BTX–negative region outside the cell was subtracted. The average fluorescence intensity values were calculated for randomly chosen cells for each experimental condition.

***Western Blot***. The α7 antibody used (27), was generously provided by Dr. Cecilia Gotti (CNR Neuroscience Institute, Milan, Italy).

Transfected cells were harvested with PBS and lysed in RIPA buffer (10 mM Tris, pH=7.5, 150 mM NaCl, 2 mM sodium ortho-vanadate, 0,1% SDS, 1% Igepal, 1% sodium deoxycholate) in the presence of proteases inhibitors (PMSF and protease inhibitor cocktail). Equal amounts of

proteins (30 µg) were separated on SDS-PAGE and transferred to nitrocellulose. The blots were blocked overnight in 5% nonfat milk and 0.3% Tween 20 in Tris-buffered saline solution at 4°C and incubated for 2 hours with the α7 primary antibody (1-2.5 µg/ml) in 2,5% nonfat milk and 0.15% Tween 20 Tris-buffered saline solution. Immunocomplexes were revealed by chemiluminescence using 1:1000 dilution of horseradish peroxidase-conjugated appropriate secondary antibody (Amersham Biosciences GE Healthcare, Little Chalfont, England). Chemiluminescence detection was performed using an enhanced detection solution (1,25 mM luminol, 0,2 mM *p*-coumaric acid 0,06% (v/v) hydrogen peroxide, 100 mM Tris-HCl pH8,8). Immunoblots were exposed to autoradiographic film (Thermo Scientific, Waltham, MA).

***Single-channel recordings.*** Single-channel recordings were obtained in the cell-attached patch configuration (31). The bath and pipette solutions contained 142 mM KCl, 5.4 mM NaCl, 1.8 mM CaCl2, 1.7 mM MgCl2 and 10 mM HEPES (pH 7.4). For potentiation, 1 µM PNU-120596 was added to the pipette solution with ACh (12).

Single-channel currents were digitized at 5-10 µs intervals, low-pass filtered at a cut-off frequency of 10 kHz using an Axopatch 200B patch-clamp amplifier (Molecular Devices Corp.,CA). Single-channel events were idealized by the half amplitude threshold criterion using the program QuB 2.0.0.28 (https://www.qub.buffalo.edu) with a digital low-pass filter at 9 kHz. A filter of 3 kHz was used in recordings with PNU-120596 to facilitate the analysis. The open and closed time histograms obtained from idealization were fitted by the maximum interval likelihood (MIL) function in QuB (56, 57), with a dead time of 0.03-0.1 ms. This analysis was performed on the basis of a kinetic model whose resulting probability density function curves properly fit the histograms following the maximum likelihood criteria. For α7, this analysis was done by sequentially adding an open and/or closed state to a starting C↔O model in order to properly fit the corresponding histograms. Final models contained five-six closed states and three-four open states for α7 in the presence of ACh plus PNU-120596, or three closed states and one-two open states for α7 in the presence of ACh alone (31, 32, 34).

Clusters were identified as a series of closely separated openings preceded and followed by closings longer than a critical duration. Different critical closed times were calculated by MIL between each closed component. Critical times between the third and fourth closed components for α7 in the presence of PNU-120596 (~30 to 60 ms) were selected in QuB to chop the idealized data and create a sub-data set that only contained clusters to define mean cluster duration.

***Electrical fingerprinting strategy.*** To define amplitude classes from receptors generated by co-expression of high and low conductance subunits, all clusters were selected regardless of their current amplitudes. Amplitude histograms were then constructed, and the different amplitude classes were distinguished. The number of amplitude classes and the mean cluster duration for each class were determined by the X-means algorithm included in the QuB software. Although up to 4 different amplitude classes were detected using the X-means algorithm, not all recordings contain events of all classes. Open time histograms were determined as described above for a selected amplitude class.

Results with QuB analysis were similar to those obtained with TAC and TAC fit programs (Bruxton corporation, Seattle, WA) as described before (12, 24, 25). Briefly, events were detected by the half amplitude threshold criterion using the program TAC. To define amplitude classes, analysis was performed by tracking events regardless of current amplitude. Amplitude histograms were then constructed and fitted by TAC fit. The different amplitude classes were distinguished by this way in experiments shown in Fig. 4.

***Statistical analysis***. Unless otherwise noted, data were presented as mean ± SD. Statistical comparisons were done using pairwise t test or one-way ANOVA with GraphPad Prism (GraphPad Software Inc.). Statistically significance difference was established at p-values<0.05.

***Molecular Modelling.*** A homology model for the extracellular region of human α7 receptor was created based on the structure of the α7-AChBP chimera (PDB code: 5AFM). The amino acid sequence for the human α7 subunit (accession number: CAD88995.1) was aligned and modeled using MODELLER 9v8 (58). Ten models were generated; of these, the one with the lowest energy

and the smallest percentage of amino acid residues in the disallowed region of the Ramachandran plot was selected. To obtain a 3D model of dupα7 we used the I-TASSER server (https://zhanglab.ccmb.med.umich.edu/I-TASSER/, (45)). This server performs structure and function prediction for a query amino acid sequence by a combination of homology modeling, threading and ab initio modeling. Five models were generated, and the best model was selected on the base of the C-score. Structure analysis and figures were generated using Discovery Studio Visualizer v4.5 suite (Dassault Systemes BIOVIA, San Diego).

**Acknowledgments:** NACHO and BOSC-23 cells were generously provided by Dr. Sine (Mayo Clinic); α7 antibody was generously provided by Dr. Cecilia Gotti. Our special thanks to Dr. Leonardo Dionisio for contributing to the early stages of this project.

**Conflict of interest:** The authors declare that they have no conflicts of interest with the contents of this article.

**References**


1. Corringer, P.-J., Poitevin, F., Prevost, M. S., Sauguet, L., Delarue, M., and Changeux, J.-P. (2012) Structure and Pharmacology of Pentameric Receptor Channels: From Bacteria to Brain. *Structure*. **20**, 941–956
2. Sauguet, L., Shahsavar, A., Poitevin, F., Huon, C., Menny, A., Nemecz, A., Haouz, A., Changeux, J.-P., Corringer, P.-J., and Delarue, M. (2014) Crystal structures of a pentameric ligand-gated ion channel provide a mechanism for activation. *Proc. Natl. Acad. Sci.* **111**, 966–971
3. Morales-Perez, C. L., Noviello, C. M., and Hibbs, R. E. (2016) X-ray structure of the human α4β2 nicotinic receptor. *Nature*. **538**, 411–415
4. Lendvai, B., Kassai, F., Szájli, A., and Némethy, Z. (2013) α7 Nicotinic acetylcholine receptors and their role in cognition. *Brain Res. Bull.* **93**, 86–96
5. Corradi, J., and Bouzat, C. (2016) Understanding the Bases of Function and Modulation of alpha 7 Nicotinic Receptors: Implications for Drug Discovery. *Mol. Pharmacol.* **90**, 288–299
6. Sinkus, M. L., Graw, S., Freedman, R., Ross, R. G., Lester, H. A., and Leonard, S. (2015) The human CHRNA7 and CHRFAM7A genes: A review of the genetics, regulation, and function. *Neuropharmacology*. **96**, 274–288
7. Bouzat, C., Gumilar, F., Spitzmaul, G., Wang, H.-L., Rayes, D., Hansen, S. B., Taylor, P., and Sine, S. M. (2004) Coupling of agonist binding to channel gating in an ACh-binding protein linked to an ion channel. *Nature*. **430**, 896–900
8. Lee, W. Y., and Sine, S. M. (2005) Principal pathway coupling agonist binding to channel gating in nicotinic receptors. *Nature*. **438**, 243–7
9. Bartos, M., Corradi, J., and Bouzat, C. (2009) Structural Basis of Activation of Cys-Loop Receptors: the Extracellular–Transmembrane Interface as a Coupling Region. *Mol. Neurobiol.* **40**, 236–252
10. Sine, S. M. (2012) End-plate acetylcholine receptor: structure, mechanism, pharmacology, and disease. *Physiol. Rev.* **92**, 1189–234
11. Bouzat, C., Lasala, M., Nielsen, B. E., Corradi, J., and Esandi, M. del C. (2017) Molecular function of α7 nicotinic receptors as drug targets. *J. Physiol.* 10.1113/JP275101
12. Andersen, N., Corradi, J., Sine, S. M., and Bouzat, C. (2013) Stoichiometry for activation of neuronal α7 nicotinic receptors. *Proc. Natl. Acad. Sci. U. S. A.* **110**, 20819–20824
13. Sinkus, M. L., Lee, M. J., Gault, J., Logel, J., Short, M., Freedman, R., Christian, S. L., Lyon, J., and Leonard, S. (2009) A 2-base pair deletion polymorphism in the partial duplication of the α7 nicotinic acetylcholine gene (CHRFAM7A) on chromosome 15q14 is associated with schizophrenia. *Brain Res.* **1291**, 1–11
14. Riley, B., Williamson, M., Collier, D., Wilkie, H., and Makoff, A. (2002) A 3-Mb map of a large Segmental duplication overlapping the alpha7-nicotinic acetylcholine receptor gene (CHRNA7) at human 15q13-q14. *Genomics*. **79**, 197–209
15. Costantini, T., Dang, X., Yurchyshyna, M.V., Coimbra, R., Eliceiri, B.P., and Baird, A. (2015) A Human-Specific α7-Nicotinic Acetylcholine Receptor Gene in Human Leukocytes: Identification, Regulation and the Consequences of CHRFAM7A Expression. *Mol. Med.* **21**, 326-336.
16. Flomen, R. H., Shaikh, M., Walshe, M., Schulze, K., Hall, M.-H., Picchioni, M., Rijsdijk, F., Toulopoulou, T., Kravariti, E., Murray, R. M., Asherson, P., Makoff, A. J., and Bramon, E. (2013) Association between the 2-bp deletion polymorphism in the duplicated version of the alpha7 nicotinic receptor gene and P50 sensory gating. *Eur. J. Hum. Genet.* **21**, 76–81
17. Costantini, T. W., Dang, X., Coimbra, R., Eliceiri, B. P., and Baird, A. (2015) CHRFAM7A, a human-specific and partially duplicated α7-nicotinic acetylcholine receptor gene with the potential to specify a human-specific inflammatory response to injury. *J. Leukoc. Biol.* **97**, 247–257

18. Villiger, Y., Szanto, I., Jaconi, S., Blanchet, C., Buisson, B., Krause, K.-H., Bertrand, D., and Romand, J.-A. (2002) Expression of an alpha7 duplicate nicotinic acetylcholine receptor-related protein in human leukocytes. *J. Neuroimmunol.* **126**, 86–98
19. Benfante, R., Antonini, R. A., De Pizzol, M., Gotti, C., Clementi, F., Locati, M., and Fornasari, D. (2011) Expression of the α7 nAChR subunit duplicate form (CHRFAM7A) is down-regulated in the monocytic cell line THP-1 on treatment with LPS. *J. Neuroimmunol.* **230**, 74–84
20. Dang, X., Eliceiri, B. P., Baird, A., and Costantini, T. W. (2015) CHRFAM7A: A human-specific α7-nicotinic acetylcholine receptor gene shows differential responsiveness of human intestinal epithelial cells to LPS. *FASEB J.* **29**, 2292–2302
21. De Lucas-Cerrillo, A. M., Maldifassi, M. C., Arnalich, F., Renart, J., Atienza, G., Serantes, R., Cruces, J. S., Sánchez-Pacheco, A., Andrés-Mateos, E., and Montiel, C. (2011) Function of partially duplicated human α7 nicotinic receptor subunit CHRFAM7A gene: Potential implications for the cholinergic anti-inflammatory response. *J. Biol. Chem.* **286**, 594–606
22. Wang, Y., Xiao, C., Indersmitten, T., Freedman, R., Leonard, S., and Lester, H. A. (2014) The duplicated α7 subunits assemble and form functional nicotinic receptors with the full-length α7. *J. Biol. Chem.* **289**, 26451–26463
23. Araud, T., Graw, S., Berger, R., Lee, M., Neveu, E., Bertrand, D., and Leonard, S. (2011) The chimeric gene CHRFAM7A, a partial duplication of the CHRNA7 gene, is a dominant negative regulator of α7 nAChR function. *Biochem. Pharmacol.* **82**, 904–914
24. Rayes, D., De Rosa, M. J., Sine, S. M., and Bouzat, C. (2009) Number and Locations of Agonist Binding Sites Required to Activate Homomeric Cys-Loop Receptors. *J. Neurosci.* **29**, 6022–6032
25. Andersen, N., Corradi, J., Bartos, M., Sine, S. M., and Bouzat, C. (2011) Functional relationships between agonist binding sites and coupling regions of homomeric Cys-loop receptors. *J. Neurosci.* **31**, 3662–3669
26. daCosta, C. J. B., Free, C. R., and Sine, S. M. (2015) Stoichiometry for α-bungarotoxin block of α7 acetylcholine receptors. *Nat. Commun.* **6**, 8057
27. Gotti, C., Briscini, L., Verderio, C., Oortgiesen, M., Balestra, B., and Clementi, F. (1995) Native nicotinic acetylcholine receptors in human Imr32 neuroblastoma cells: functional, immunological and pharmacological properties. *Eur. J. Neurosci.* **7**, 2083–92
28. Chen, D., Dang, H., and Patrick, J. W. (1998) Contributions of N-linked glycosylation to the expression of a functional alpha7-nicotinic receptor in Xenopus oocytes. *J. Neurochem.* **70**, 349–57
29. Drisdel, R. C., and Green, W. N. (2000) Neuronal alpha-bungarotoxin receptors are alpha7 subunit homomers. *J. Neurosci.* **20**, 133–9
30. Tsetlin, V., Shelukhina, I., Kryukova, E., Burbaeva, G., Starodubtseva, L., Skok, M., Volpina, O., and Utkin, Y. (2007) Detection of α7 nicotinic acetylcholine receptors with the aid of antibodies and toxins. *Life Sci.* **80**, 2202–2205
31. Bouzat, C., Bartos, M., Corradi, J., and Sine, S. M. (2008) The Interface between Extracellular and Transmembrane Domains of Homomeric Cys-Loop Receptors Governs Open-Channel Lifetime and Rate of Desensitization. *J. Neurosci.* **28**, 7808–7819
32. daCosta, C. J. B., Free, C. R., Corradi, J., Bouzat, C., and Sine, S. M. (2011) Single-channel and structural foundations of neuronal α7 acetylcholine receptor potentiation. *J. Neurosci.* **31**, 13870–9
33. Hurst, R. S., Hajós, M., Raggenbass, M., Wall, T. M., Higdon, N. R., Lawson, J. A., Rutherford-Root, K. L., Berkenpas, M. B., Hoffmann, W. E., Piotrowski, D. W., Groppi, V. E., Allaman, G., Ogier, R., Bertrand, S., Bertrand, D., and Arneric, S. P. (2005) A novel positive allosteric modulator of the alpha7 neuronal nicotinic acetylcholine receptor: in vitro and in vivo characterization. *J. Neurosci.* **25**, 4396–405
34. Andersen, N. D., Nielsen, B. E., Corradi, J., Tolosa, M. F., Feuerbach, D., Arias, H. R., and

Bouzat, C. (2016) Exploring the positive allosteric modulation of human α7 nicotinic receptors from a single-channel perspective. *Neuropharmacology*. **107**, 189–200
35. Bouzat, C., and Sine, S. M. (2017) Nicotinic acetylcholine receptors at the single-channel level. *Br. J. Pharmacol.* 10.1111/bph.13770
36. Gill, J. K., Savolainen, M., Young, G. T., Zwart, R., Sher, E., and Millar, N. S. (2011) Agonist activation of α7 nicotinic acetylcholine receptors via an allosteric transmembrane site. *Proc. Natl. Acad. Sci.* **108**, 5867–5872
37. daCosta, C. J. B., and Sine, S. M. (2013) Stoichiometry for drug potentiation of a pentameric ion channel. *Proc. Natl. Acad. Sci.* **110**, 6595–6600
38. Puskar, N. L., Xiu, X., Lester, H. A., and Dougherty, D. A. (2011) Two Neuronal Nicotinic Acetylcholine Receptors, α4β4 and α7, Show Differential Agonist Binding Modes. *J. Biol. Chem.* **286**, 14618–14627
39. Gu, S., Matta, J. A., Lord, B., Harrington, A. W., Sutton, S. W., Davini, W. B., and Bredt, D. S. (2016) Brain α7 Nicotinic Acetylcholine Receptor Assembly Requires NACHO. *Neuron*. **89**, 948–955
40. Castillo, M., Mulet, J., Gutiérrez, L. M., Ortiz, J. A., Castelán, F., Gerber, S., Sala, S., Sala, F., and Criado, M. (2005) Dual role of the RIC-3 protein in trafficking of serotonin and nicotinic acetylcholine receptors. *J. Biol. Chem.* **280**, 27062–8
41. Breese, C. R., Marks, M. J., Logel, J., Adams, C. E., Sullivan, B., Collins, A. C., and Leonard, S. (1997) Effect of smoking history on [3H]nicotine binding in human postmortem brain. **282**, 7–13
42. Kabbani, N., Nordman, J. C., Corgiat, B. A., Veltri, D. P., Shehu, A., Seymour, V. A., and Adams, D. J. (2013) Are nicotinic acetylcholine receptors coupled to G proteins? *BioEssays*. **35**, 1025–1034
43. Chimienti, F., Hogg, R. C., Plantard, L., Lehmann, C., Brakch, N., Fischer, J., Huber, M., Bertrand, D., and Hohl, D. (2003) Identification of SLURP-1 as an epidermal neuromodulator explains the clinical phenotype of Mal de Meleda. *Hum. Mol. Genet.* **12**, 3017–3024
44. Locke, D. P., Jiang, Z., Pertz, L. M., Misceo, D., Archidiacono, N., and Eichler, E. E. (2004) Molecular evolution of the human chromosome 15 pericentromeric region. *Cytogenet. Genome Res.* **108**, 73–82
45. Zhang, Y. (2008) I-TASSER server for protein 3D structure prediction. *BMC Bioinformatics*. **9**, 40
46. Chatzidaki, A., and Millar, N. S. (2015) Allosteric modulation of nicotinic acetylcholine receptors. *Biochem. Pharmacol.* **97**, 408–417
47. Kelley, S. P., Dunlop, J. I., Kirkness, E. F., Lambert, J. J., and Peters, J. A. (2003) A cytoplasmic region determines single-channel conductance in 5-HT3 receptors. *Nature*. **424**, 321–324
48. Hassaine, G., Deluz, C., Grasso, L., Wyss, R., Tol, M. B., Hovius, R., Graff, A., Stahlberg, H., Tomizaki, T., Desmyter, A., Moreau, C., Li, X.-D., Poitevin, F., Vogel, H., and Nury, H. (2014) X-ray structure of the mouse serotonin 5-HT3 receptor. *Nature*. **512**, 276–281
49. Murray, T. A., Bertrand, D., Papke, R. L., George, A. A., Pantoja, R., Srinivasan, R., Liu, Q., Wu, J., Whiteaker, P., Lester, H. A., and Lukas, R. J. (2012) α7 ß2 Nicotinic Acetylcholine Receptors Assemble, Function, and Are Activated Primarily via Their α7- α7 Interfaces. *Mol. Pharmacol.* **81**, 175–188
50. Nielsen, B. E., Minguez, T., Bermudez, I. and Bouzat, C. (2018) Molecular function of the novel α7ß2 nicotinic receptor. *Cell. Mol. Life Sci.* https://doi.org/10.1007/s00018-017-2741-4.
51. Pear, W. S., Nolan, G. P., Scott, M. L. and Baltimore, D. (1993) Production of high-titer helper-free retroviruses by transient transfection. *Proc. Natl. Acad. Sci U.S.A.* **90**, 8392-8396
52. Bouzat, C., Bren, N., and Sine, S. M. (1994) Structural basis of the different gating kinetics

of fetal and adult acetylcholine receptors. *Neuron*. **13**, 1395–402
53. Bouzat, C., Roccamo, A. M., Garbus, I., and Barrantes, F. J. (1998) Mutations at lipid-exposed residues of the acetylcholine receptor affect its gating kinetics. *Mol. Pharmacol.* **54**, 146–53
54. Mazzaferro, S., Bermudez, I., Sine, S. M (2017) α4ß2 nicotinic acetylcholine receptors: Relationships between subunit stoichiometry and function at the single channel level. *J. Biol. Chem.* **292**, 2729-2740
55. Millar, N. S. (2009) RIC-3: a nicotinic acetylcholine receptor chaperone. *Br. J. Pharmacol.* **153**, S177–S183
56. Qin, F., Auerbach, A., and Sachs, F. (1997) Maximum likelihood estimation of aggregated Markov processes. *Proc. R. Soc. B Biol. Sci.* **264**, 375–383
57. Qin, F., Auerbach, A., and Sachs, F. (1996) Estimating single-channel kinetic parameters from idealized patch-clamp data containing missed events. *Biophys. J.* **70**, 264–80
58. Šali, A., and Blundell, T. L. (1993) Comparative Protein Modelling by Satisfaction of Spatial Restraints. *J. Mol. Biol.* **234**, 779–815

**FOOTNOTES**

This work was supported by grants from Universidad Nacional del Sur (UNS) (CB and MCE), Agencia Nacional de Promoción Científica y Tecnológica (ANPCYT) (CB and JC), and Consejo Nacional de Investigaciones Científicas y Técnicas (CONICET) Argentina (CB).

The abbreviations used are: nAChR, nicotinic acetylcholine receptor; α-BTX, α-bungarotoxin; PAM, positive allosteric modulator; ACh, acetylcholine; MFI, mean fluorescence intensity; PNU-120596, N-(5-Chloro-2,4-dimethoxyphenyl)-N'-(5-methyl-3-isoxazolyl)-urea; 4BP-TQS, 4-(4-Bromophenyl)-3a,4,5,9b-tetrahydro-3H-cyclopenta[c]quinoline-8-sulfonamide; TM, transmembrane.

**Table 1.** Kinetic properties of α7 and α7/dupα7 receptors.

| Subunit combination | Receptor | PAM (1 µM) | Amplitude class (pA) | $\tau_0$ (ms) | $\tau_{cluster}$ (ms) | n |
|---|---|---|---|---|---|---|
| α7 | $(\alpha7)_5$ | - | nd | 0.31 ± 0.21 | 0.39 ± 0.12 | 4 |
| α7 | $(\alpha7)_5$ | PNU-120596 | 9.8 ± 1.7 | 72 ± 41 | 1952± 548 | 5 |
| α7LC:α7 (1:4) | $(\alpha7LC)_2(\alpha7)_3$ | PNU-120596 | 6.1 ± 0.4 | 63 ± 25 | 1794 ± 1140 | 7 |
| α7LC:dupα7 (1:3) | $(\alpha7LC)_2(dup\alpha7)_3$ | PNU-120596 | 5.8 ± 0.5 | 93 ± 40 | 2195 ± 754 | 11 |

Cells expressing the specified subunit combination were used for single-channel recordings. Channels were activated by 100 µM ACh in the absence or presence of 1 µM PNU-120596. For α7, a single ~10-pA class is detected. The mean durations of open ($\tau_o$) and clusters ($\tau_{cluster}$) were obtained from the corresponding histograms.
Channel events from $(\alpha7LC)_2(dup\alpha7)_3$ and $(\alpha7LC)_2(\alpha7)_3$ heteromeric receptors correspond to the 6-pA amplitude class recorded from cells transfected with dupα7 and α7LC or α7 and α7LC, respectively (Fig. 4E). The differences of durations among all receptors were not statistically significant (p= 0.23 for $\tau_o$ and 0.62 for $\tau_{cluster}$, one-way ANOVA). nd: not determined.

***Figures***

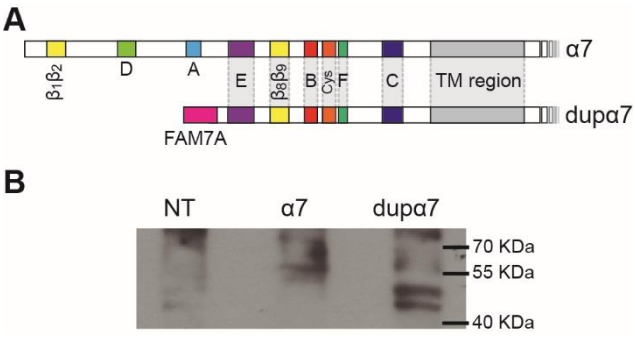


***Figure 1. dupα7 subunit***

A. Diagram of α7 and dupα7 subunits, showing the loops that form the ACh binding site (Loops A-F); loops at the coupling region ($\beta_1\beta_2$, Cys and $\beta_8\beta_9$ loops); the transmembrane (TM) region; and the FAM7A part of dupα7 at the N-terminal domain.
B. Expression of dupα7 on BOSC-23 cells. Lysates of BOSC-23 cells transfected with α7 or dupα7 cDNA were probed by Western blotting for the subunit protein. NT: corresponds to lysates from non-transfected cells.

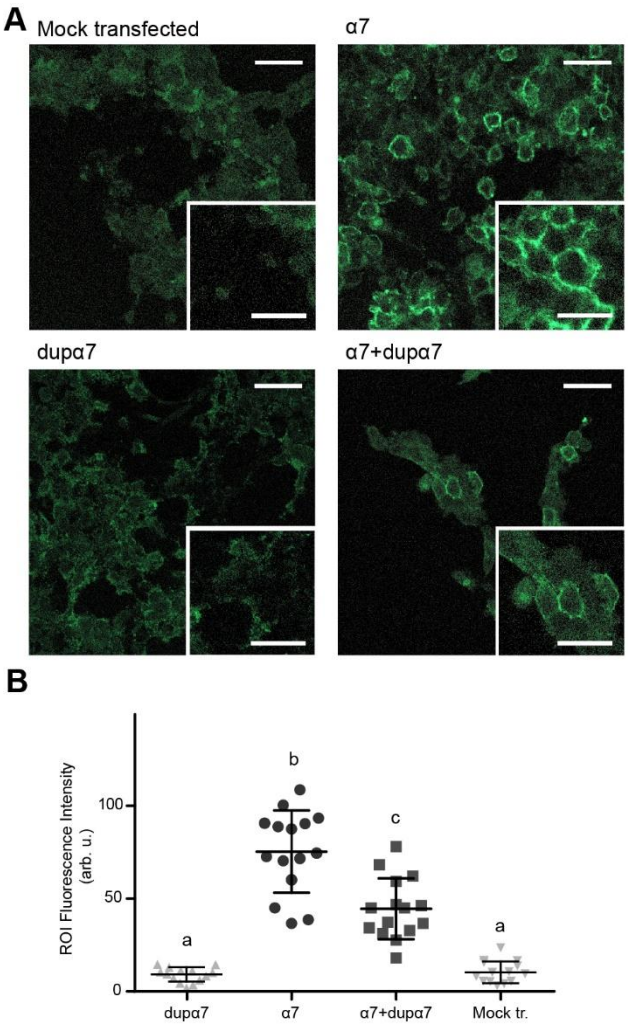


***Figure 2. α-BTX labeling of BOSC cells transfected with a7 and/or dupa7.***
Cells were transfected with α7 cDNA, dupα7 cDNA or with the combination 1:3 α7:dupα7 cDNA. Mock transfected cells correspond to cells transfected with irrelevant plasmid DNA. The total amount of DNA per transfection was normalized with the addition of irrelevant plasmid DNA.
A. Representative confocal microscopy images showing the membrane fluorescence signal generated in transfected cells stained with Alexa Fluor 488-labeled α-BTX. A zoomed image is included at the lower right corner of each panel. Scale bars correspond to 40 μm for the non-zoomed images and 20 μm for the zoomed images. B. Scatter plot of fluorescence intensity in the region of interest (ROI) of individual transfected cells. Results are expressed as mean ± SD (n=15). Different letters (a-c) denote statistically significant differences among groups ($p<0.0001$; Sidak's multiple comparisons test).

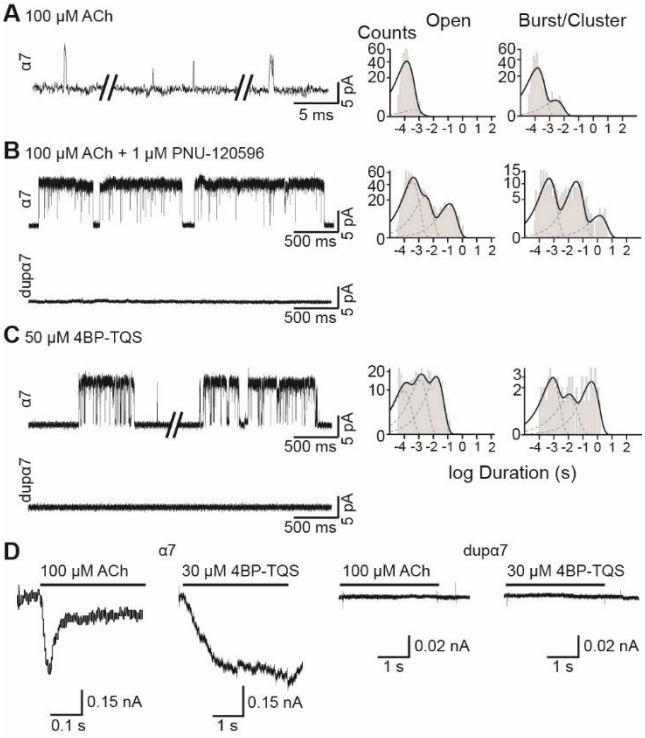


***Figure 3. Functional responses of α7 or dupα7.***

BOSC-23 cells were transfected with α7 or dupα7 cDNAs together with NACHO and Ric-3 as described in Methods.

A. Representative single-channel currents activated by 100 μM ACh from cells transfected with α7. Typical open and burst duration histograms are shown.

B. Representative traces of ACh-elicited single-channel currents in the presence of 1 μM PNU-120596 from cells transfected with α7 (top) or dupα7 cDNAs (bottom). Typical open and cluster duration histograms are shown for α7.

C. Single channel currents activated by the allosteric agonist, 4BP-TQS (50 μM) from cells transfected with α7 (top) or dupα7 cDNAs (bottom). Typical open and cluster duration histograms are shown for α7.

Membrane potential: -70 mV. Filter: 9 kHz for ACh and 3 kHz for ACh and PNU-120596 or 4BP-TQS. Openings are shown as upward deflections.

In all histograms, dashed grey lines correspond to individual components; and black lines correspond to the sum of components.

D. Macroscopic currents activated by 100 μM ACh or 30 μM 4BP-TQS from cells transfected with α7 or dupα7 cDNAs. No currents from dupα7-expressing cells were elicited by the allosteric agonist.

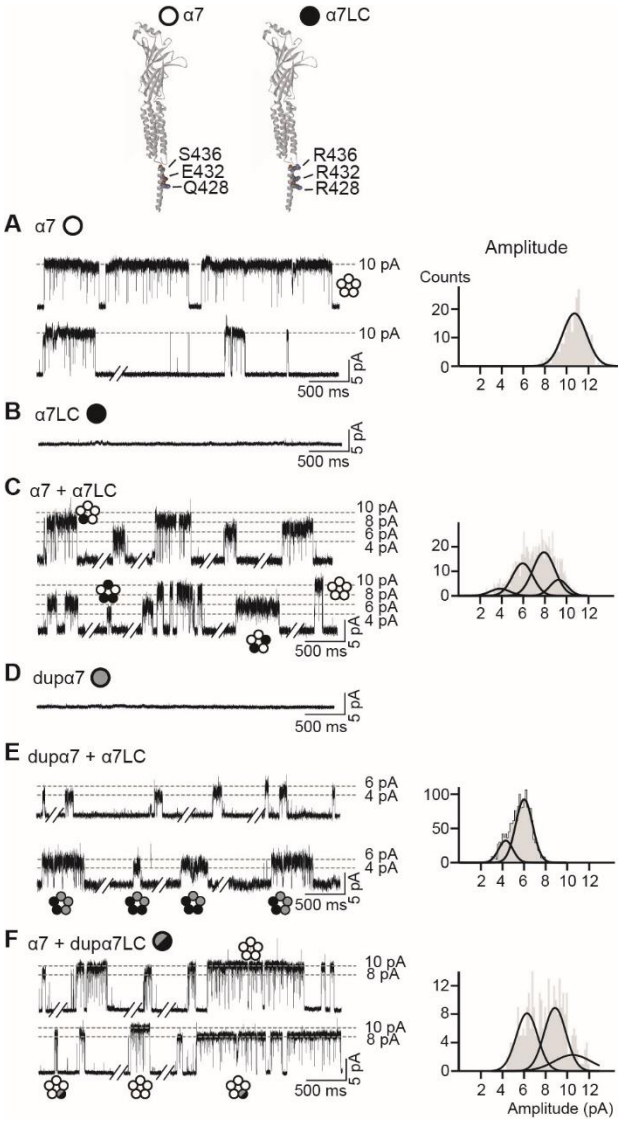


***Figure 4. Electrical Fingerprinting for α7/α7LC and dupα7/α7LC heteromeric receptors.***
Top: Models showing the different amino acid residues at the intracellular region for α7 and α7LC. Left panels: Representative single-channel currents activated by 100 μM ACh + 1 μM PNU-120596 from cells expressing α7 (A), α7LC (B), α7 + α7LC (C), dupα7 (D), dupα7 + α7LC (E), and dupα7LC + α7 (F). The traces for the mixed subunit conditions are excerpts from the same recording. Membrane potential: -70 mV. Filter: 3 kHz. Channel openings are shown as upward deflections. The dashed lines indicate the amplitude of the different amplitude classes.
Right panels: Typical amplitude histograms for a whole recording constructed with events longer than 1 ms are shown with the fitted components.

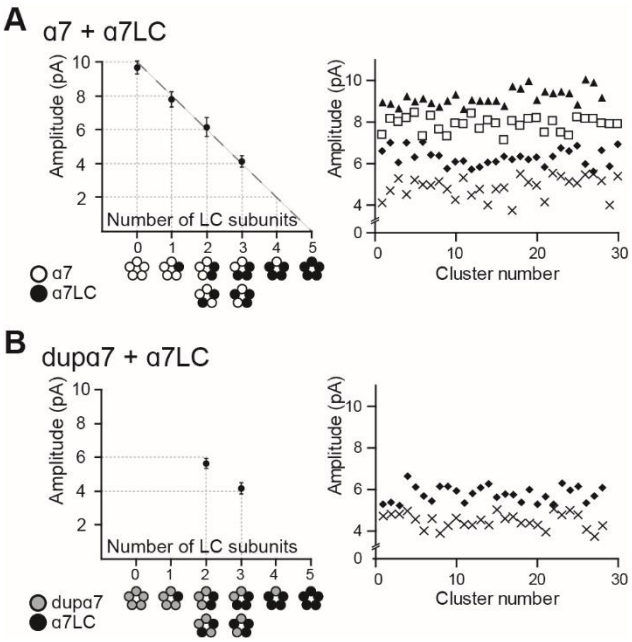


***Figure 5. Amplitude classes for the combinations α7/α7LC and dupα7/α7LC.***
Analysis of the amplitude classes for cells transfected with α7LC and α7 (A) or dupα7 (B) cDNAs.
*Left:* A. Plot of mean current amplitude against the number of α7LC subunits in the pentameric arrangement for the α7/α7LC combination. The fitted slope by least-squares method is 1.81 ± 0.06 pA/ LC subunit. Data are plotted as mean ± SD of n=7 for amplitude class of 10, n=10 for amplitude classes of 8 pA and 6 pA, and n=8 for the amplitude class of 4 pA.
B. Plot of mean current amplitude against the number of α7LC subunits in the pentameric arrangement for the α7LC/dupα7 combination. The fitted slope by least-squares method is 1.63 ± 0.3 pA/ LC subunit. Data are plotted as mean ± SD of n=15 for amplitude class of 6 and n=3 for the amplitude class of 4 pA.
Right: Representative dot plots showing the distribution of clusters as a function of their mean amplitude. Recordings were obtained from cells transfected with α7/α7LC (A) or dupα7/α7LC (B). Each plot corresponds to a single recording, and each point, to a single cluster. The number of amplitude classes was determined by the X-means algorithm included in the QuB software.

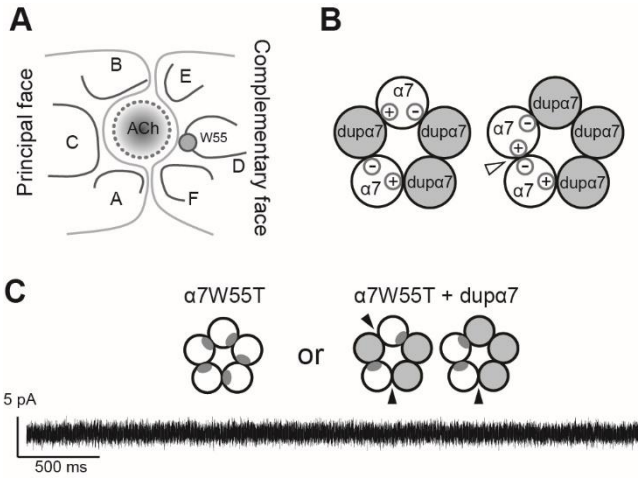


***Figure 6. Requirements for $(\alpha 7)_2(dup\alpha 7)_3$ channel activation.***

A. Diagram showing the α7 binding site for ACh. Mutations were introduced at the complementary face (W55T).

B. Possible subunit arrangements of receptors containing three dupα7 and two α7 subunits. The arrow shows the functional α7/α7 interfacial binding site.

C. Representative single-channel recordings in the presence of 100 μM ACh + 1 μM PNU-120596 showing the lack of channel activity in cells transfected with dupα7 and α7W55T cDNA. The black arrows show possible ACh binding sites in which the complementary face is provided by dupα7. Membrane potential: -70 mV. Filter: 3 kHz.

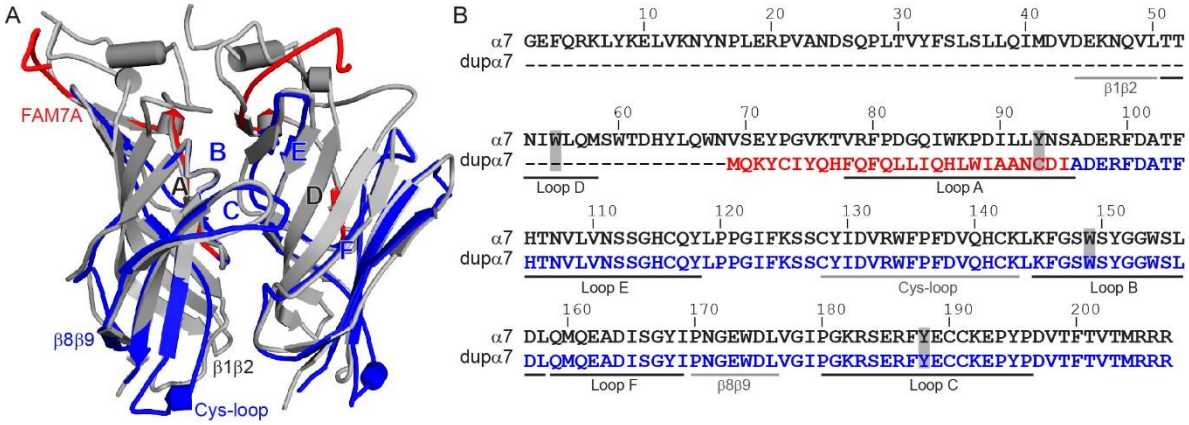


***Fig. 7. Superimposed molecular models of dupα7 and α7.***

A. Structural alignment of extracellular domains of two adjacent α7/α7 and dupα7/dupα7 subunits. Human α7 structural model was created by homology modelling based on the structure of the α7-AChBP chimera (PDB code: 5AFM) and the 3D model of dupα7 was generated by the I-TASSER server (See Methods). The α7 subunits are shown in grey. In dupα7 subunits the region corresponding to FAM7A is shown in red and that corresponding to α7, in blue. Binding and interface loops present in both molecules are indicated with blue letters and those present in α7 but absent in dupα7, with black letters.

B. Alignment of the α7 and dupα7 sequences (accessions numbers CAD88995 and NP_647536). The α7 sequence does not include the signal peptide. The sequences are identical after amino acid residue 95 of α7. dupα7 sequence corresponding to the FAM7A region is in red. Residues for the six binding loops (A-F) and loops at the coupling region are indicated with black and grey lines, respectively. Aromatic residues reported as essential for α7 agonist response are in grey boxes.

# A human-specific, truncated α7 nicotinic receptor subunit assembles with full-length α 7 and forms functional receptors with different stoichiometries

Matías Lasala, Jeremías Corradi, Ariana Bruzzone, María del Carmen Esandi and Cecilia Bouzat

*J. Biol. Chem. published online May 21, 2018*

---